

The potential for grain refinement of a super austenitic stainless steel with a cerium grain refiner

Kerstin Baumgartner¹, Christian Bernhard¹, Peter Presoly¹, Martin Hafok², Harald Leitner² –

¹ Montanuniversität Leoben - Chair of Ferrous Metallurgy, Leoben, Austria; ² Böhler Edelstahl GmbH & Co KG, Kapfenberg, Austria

Austenitic stainless steels typically show a tendency towards the formation of large columnar grains and shrinking porosities during solidification. Altering this primary structure to be finer normally leads to improved mechanical properties in the final product. This can be achieved by applying grain refiners to cause a columnar to equiaxed transition at an early stage of solidification, resulting in a fine grained equiaxed microstructure in the center of the ingot.

The influence of a commercial grain refiner containing Fe-Cr-Si-Ce on the super austenitic stainless steel X1CrNiMoCuN20-18-7 was investigated. From extensive literature research, AlCeO_3 and Ce_2O_3 were identified as most promising particles for the heterogeneous nucleation of austenite. From the result of thermodynamic considerations the activities of O, Al and Ce were then adjusted to guarantee for stable AlCeO_3 or Ce_2O_3 particles. In melting experiments a two stage deoxidation practice in the induction furnace prior to casting of the 20 kg ingots resulted in a precocious columnar to equiaxed transition. This paper deals with a detailed SEM/EDS investigation of the inclusions, macro- and microetching of the ingots and the quantitative analysis of the formed microstructure.

KEYWORDS: SUPER AUSTENITIC STEEL – GRAIN REFINEMENT – SOLIDIFICATION STRUCTURE
– CERIUM – HETEROGENEOUS NUCLEATION

INTRODUCTION

In the group of stainless steels austenitic stainless steels make up the largest part. They are more costly through to the high content in chromium and nickel, but exhibit a better behavior considering formability and weldability. Super austenitic stainless steels show an even higher content in chromium and nickel additionally they are alloyed with molybdenum and nitrogen. Therefore they achieve a better resistance to pitting corrosion and stress corrosion cracking [1].

Grain size is an important material property as it influences tensile strength and ductility [2,3]. Smaller grains can lead to higher resistance against stress corrosion cracking and hydrogen embrittlement [4]. Fully austenitic steels show no phase transformation thus the size of the primary grains is of great importance to achieve a fine microstructure [5].

A refined cast structure can be achieved through inoculation. The activation energy for stable steel nuclei is reduced by heterogeneous nucleation sites. This makes a fine-grained, globular and undirected solidification structure possible [6]. The most important starting points for heterogeneous nucleation are exogenous nonmetallic inclusions (NMI). For a successful inoculation NMI have to fulfill the following points. First, the nuclei need a similar crystallographic structure as the primary solidifying steel phase. Second, inclusions need to be undissolvable and solid until the melt starts to solidify, also their melting point has to be higher than the metals. Third, a good wettability between the inclusion and the primary steel phase is necessary as well. Fourth, to prevent them from separating from the melt the density of liquid metal and inclusion should be similar. Fifth, the nuclei must be fine and evenly distributed in the whole melt. Such a distribution is most likely if the nuclei are products of a dissolved element in the steel and a element provided by inoculation [7]. The planar lattice registry δ is a measure for the crystallographic correspondance between nuclei and steel should be less than 15 % [8]. The undercooling of the melt, which is an indicator for the needed energy for nucleation, increases with higher δ . This means low undercooling of the melt is a sign that potent nuclei are present in the melt. Fig. 1 shows the correlation between planar

disregistry of different NMI and the possible undercooling of the melt [9]. It suggests that rare-earth oxides can act as nucleation sites for steel. At roomtemperature δ is 11 % for Ce_2O_3 and for $AlCeO_3$ it decreases further to 5 % [10].

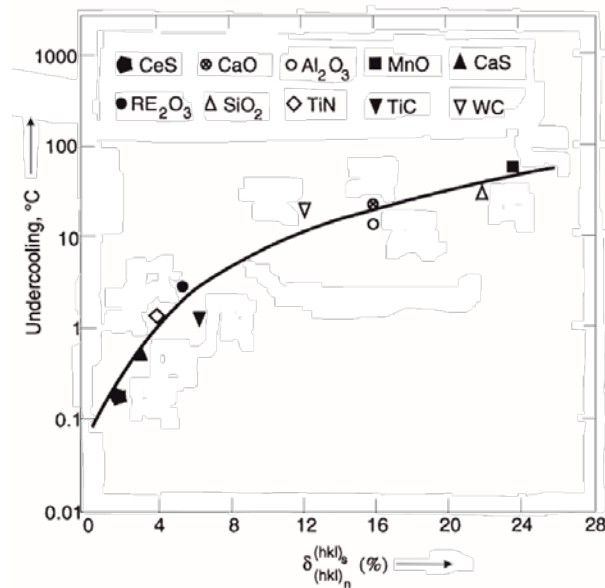


Fig. 1 - Relationship between planar lattice disregistry and undercooling for different nuclei in steel [9]

The grain refining effect of rare-earth elements is reported in various publications. In labor scale experiments cerium-oxides lead to a precocious transition from columnar to equiaxed solidification [11,12]. In 20 t ingots of plain carbon steel treated with rare-earth metals the primary dendrite arm spacing and length are decreased, the growth direction is less oriented and microsegregation of C, S, P, Si and Mn is lessend [13], but also a larger globular zone together with a smaller macrosegregation is visible [14]. Van der Ejik et. al. report of finer secondary arm spacing in X1CrNiMoCuN20-18-7 when comparing the effect of commercially available Mischmetal and a similar grain refiner as used in this work [5].

Following the above Ce_2O_3 and $CeAlO_3$ were identified as favorable NMI for grain refinement. The density of cerium-oxides is nearly equal to the density of liquid steel, thus they are not able to separate due to flotation. To achieve a homogenous inclusion distribution the dissolved oxygen in the liquid steel shall react with cerium provided by inoculation. Elkems Grain Refiner – StainSeed (EGR) was applied to alloy cerium. Fig. 2 suggests a rather large stability area for Ce_2O_3 in a 10%Ni-20%Cr-Fe system. Only combining extremely low cerium contents and higher aluminum contents will lead to $AlCeO_3$.

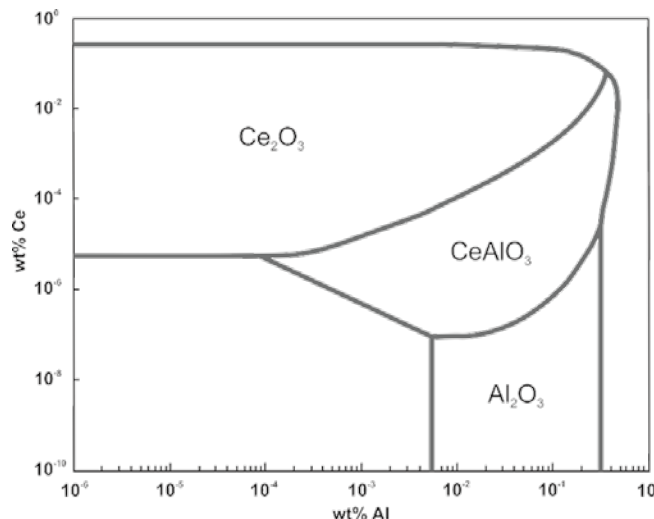


Fig. 2 - Phase stability diagram at 1550 °C in Ce-Al-100(ppm)O-Fe-20%Cr-10%Ni system: maximum dissolved oxygen amount is limited to 100 ppm [15]

EXPERIMENTAL

Grain refining experiments were performed in the melting shop of the chair of ferrous metallurgy. An open induction furnace with a maximum-capacity of 20 kg and MgO lining was used. The experiments took place according to the sequence in Fig. 3. The stainless steel X1CrNiMoCuN20-18-7 provided by Böhler Special Steel was melted as first step. The steel analysis is shown in Tab. 1. The steel composition was controlled by OES and a loss of aluminum, chromium and manganese was detected. Chromium and manganese levels in the steel melt were adjusted to meet the original steel composition. To ensure enough oxygen in the melt for cerium to react with and form the favorable NMI only 0.023 mass-% of aluminum was added to the melt shortly before EGR. Three experiments with different amounts of EGR were performed. A high loss of cerium due to oxidation was anticipated, so rather large quantities were added to guaranty for Ce_2O_3 or $CeAlO_3$ to form. The cerium amount added to the melt was as high as 0.19, 0.26 and 0.32 mass-%. For the chemical analysis of the grain refiner see Tab. 2.

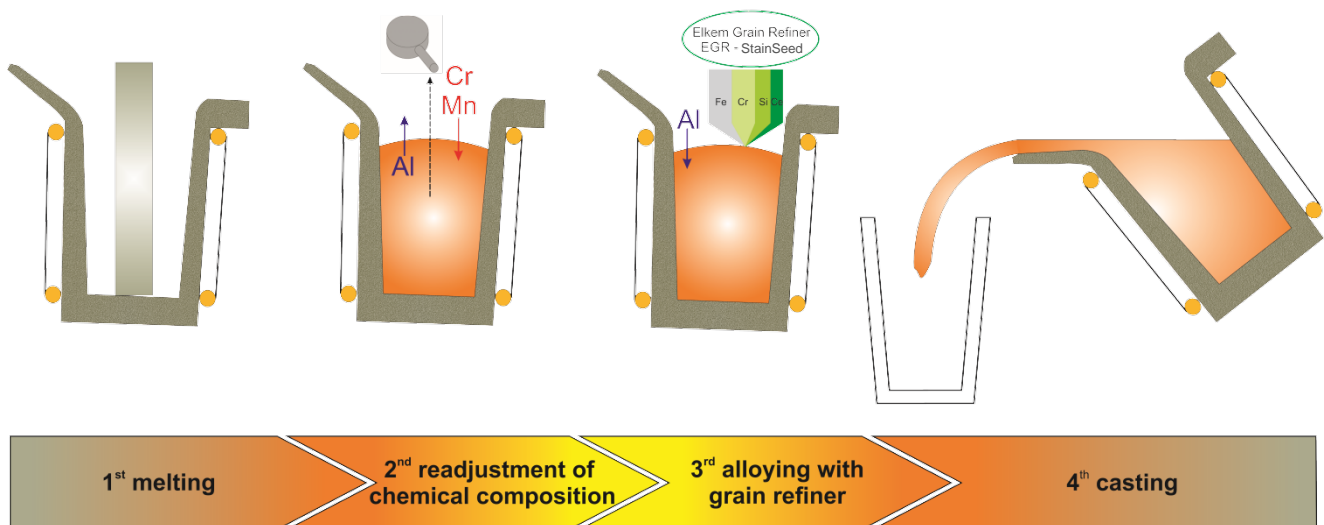


Fig. 3 - Experimental sequence

Tab. 1 - Chemical composition of X1CrNiMoCuN20-18-7 in mass-%

C	Si	Mn	Cr	Mo	Ni	N
max. 0.02	0.18	0.65	20.30	6.30	17.80	0.20

Tab. 2 - Chemical composition of EGR in mass-%

Si	Cr	Ce	C	Fe
19	33	13	0.1	balance

For the metallographic observations an optical light microscope Polyvar Pol with image analysis software Clemex Vision 4.0 and a SEM Quanta 200 Mk2 was used. Macroscopic investigations were carried out with the help of high resolution photographs. Etching took place with B-etching (= 50 ml H_2O + 5 ml konz. HNO_3 + 5 ml 30% H_2O_2 + 0.5 g $CuCl_2$). This method led to a good visibility of macro- and microstructure.

Two specimens were taken from every ingot to investigate the grain size and area percentage of equiaxed solidification as well as the microstructure. The grain size was determined by the linear intercept method. For the area part of unidirectional solidification the lengths of columnar dendrites were measured (see Fig. 4). The breadth b of the ingots is 80 mm and formula (1) is used to calculate the globular area.

$$f_{\text{glob}} = 100 \cdot \left(1 - \frac{\frac{n}{\sum_{i=1}^n 1/l_i}}{b/2} \right) \quad (1)$$

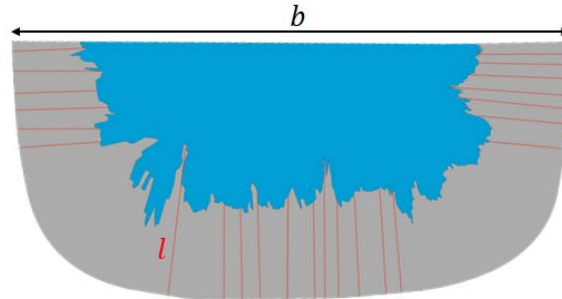


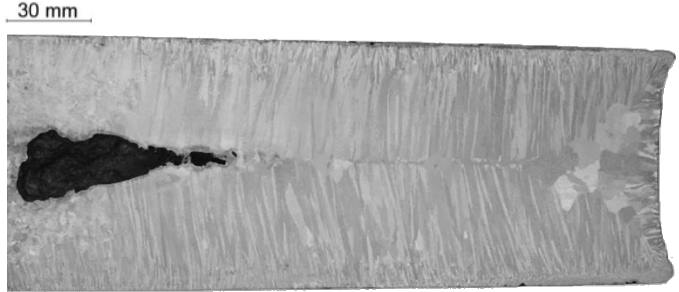

Fig. 4 - Sketch for the determination of globular solidification area

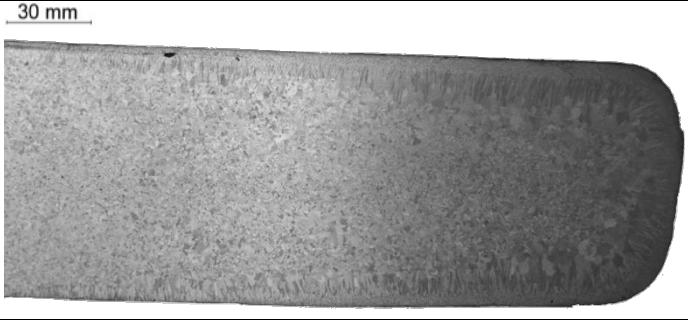
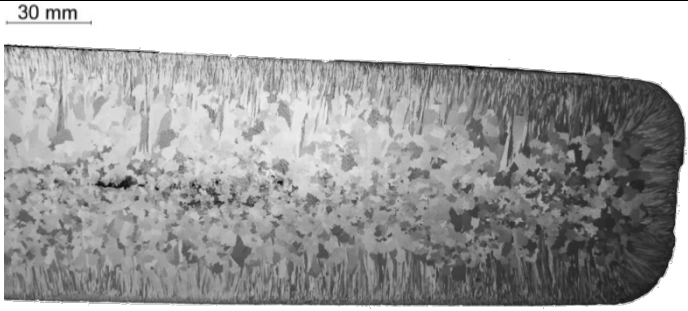
RESULTS & DISCUSSION

Influence of grain refiner on the solidification structure

The macrostructure of the ingots was severely influenced by the addition of EGR. Tab. 3 holds the comparison of the three experiments performed for this investigation and ingot 0 which was casted in a previous test series [16]. Ingot 0 shows a fully directional solidification with large primary grains and a severe shrinking porosity. Ingots 1 to 3 all have an improved macrostructure with various degrees of grain refinement. The finest grains with 1.2 mm and largest globular zone (76 %) are both visible in ingot 2. Some small shrinking porosities appeared in the treated ingots as well, but these are in a tolerable size. Apparently neither the amount of original cerium added to the melt nor the yield of cerium points directly to which ingot forms the finest as-cast structure.

Tab. 3 - Macroscopic structure and overview of experiments

Ce alloyed [mass-%]	Ce yield [mass-%]	Macro structure	Grain-size [mm]	$f_{\text{glob}} \pm \text{SD}$ [%]
Ingot 0 [16]				
No Ce added	-		-	0
Ingot 1				
0.26	0.019		5.5	40 ± 10.6

Ce alloyed [mass-%]	Ce yield [mass-%]	Macro structure	Grain-size [mm]	$f_{glob} \pm SD$ [%]
Ingots				
Ingot 2				
0.19	0.032		1.2	76 ± 5.7
Ingots				
Ingot 3				
0.32	0.073		2.8	66 ± 7.9

The examination of the microstructure by light microscopy shows that all three experiments established an equiaxed, dendritic structure in the center. The finest dendrite arms are visible in ingot 1 and 3, see Fig. 5 a) and c). In ingot 2 the dendritic structure seems coarser (Fig. 5 b)). Ingot 2 has the smallest grain size and earliest columnar to equiaxed transition, so there are more nucleation points expected in this experiment. It seems that when there are so many starting points in competition with each other, no orderly dendritic, equiaxed structure is formed and the primary dendrite arms get thicker.

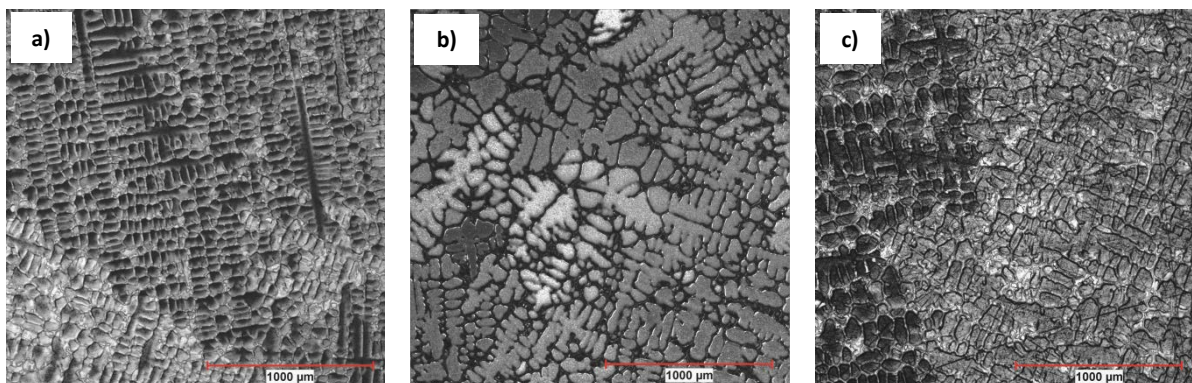


Fig. 5 – Microstructure in the ingot center – a) ingot 1; b) ingot 2; c) ingot 3

Inclusion chemistry and density by SEM-EDS measurements

SEM-EDS analysis showed that various inclusions appear in the samples, all of them contain cerium in different amounts. In Fig. 6 a) to c) the inclusions found in ingots 2 and 3 can be seen. Through the high atomic weight of cerium most of the NMI show up bright in a dark steel matrix. Most of the small inclusions have chemical compositions following $CeAlO_3$ or Ce_2SiO_5 . But there are also more complex NMI with at least two phases, a lighter phase, which has a $CeAlO_3$ composition, and a darker phase containing cerium, chromium, silicon and oxygen. As these complex inclusions mostly appear between the dendritic arms in the remaining melt it is assumed that they do not contribute to any grain refining mechanisms. Ingot 1

contains different inclusions too, shown in Fig. 6 d) to f). There were many small dark inclusions and less bright inclusions. The small dark inclusions were mixed oxides containing silicon, chromium, cerium and oxygen. Additionally there also were two-phase inclusions in the matrix containing Ce_2SiO_5 and a mixed oxide of Si, Mn, Cr, Fe, Ce and O. It appears that there are fewer inclusions with the favorable composition of $CeAlO_3$ in ingot 1 than there are in ingot 2 and 3.

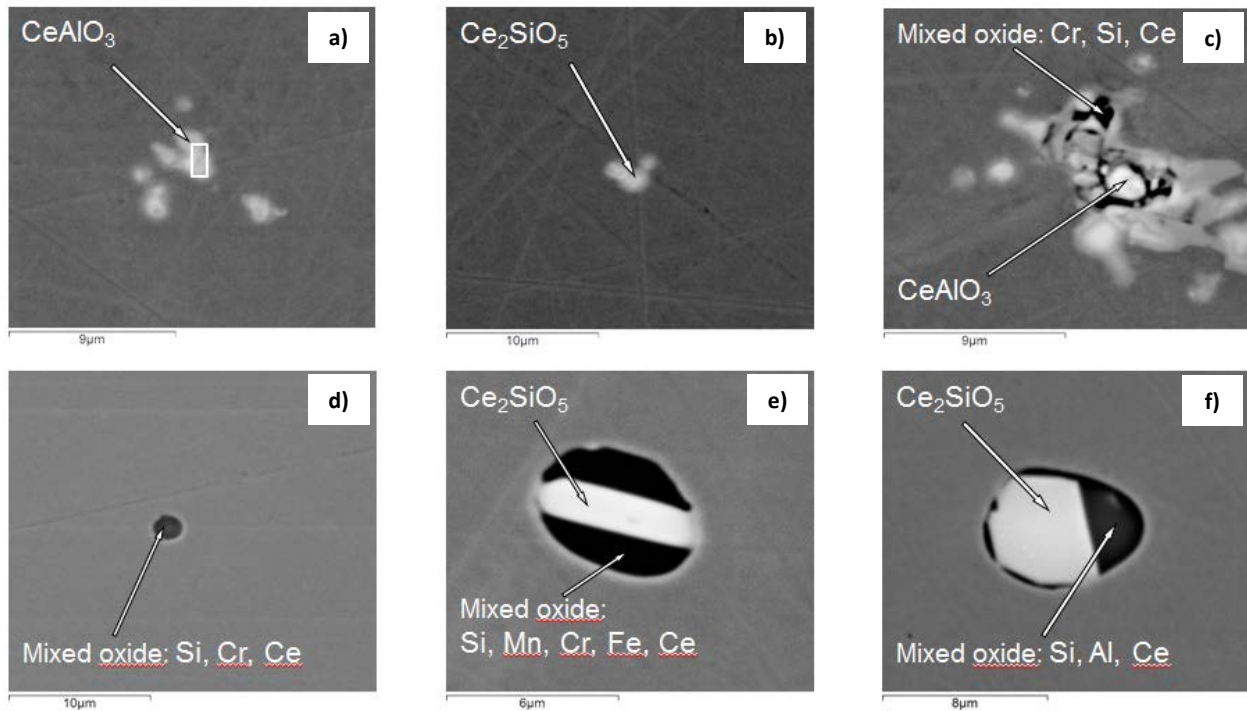


Fig. 6 - Nonmetallic inclusions investigated by SEM-EDX (a-c) ingot 2 and 3; d-f) ingot 1)

By examining the equivalent circle diameter (ECD) of the NMI the dark inclusions turn out to be generally larger than the bright ones. Fig. 7 shows box-whisker diagrams of the ECDs. The small square is the mean ECD, 25 % of the values lie below the lowest line, 50 % below the middle and 75 % below the upper line. The crosses mark 1 and 99 % of the values. The dotted line marks the 1 μm limit, this is important because only NMI smaller than 1 μm are considered as possible nucleation sites [7]. It is evident that there were no dark inclusions detected in ingot 2, whereas they appear in ingot 1 and 3 and their ECD values are spread over a broad range. In all ingots inclusions with a low disregistry to austenite and with ECD values smaller than 1 μm are available and so they also should be active for grain refinement.

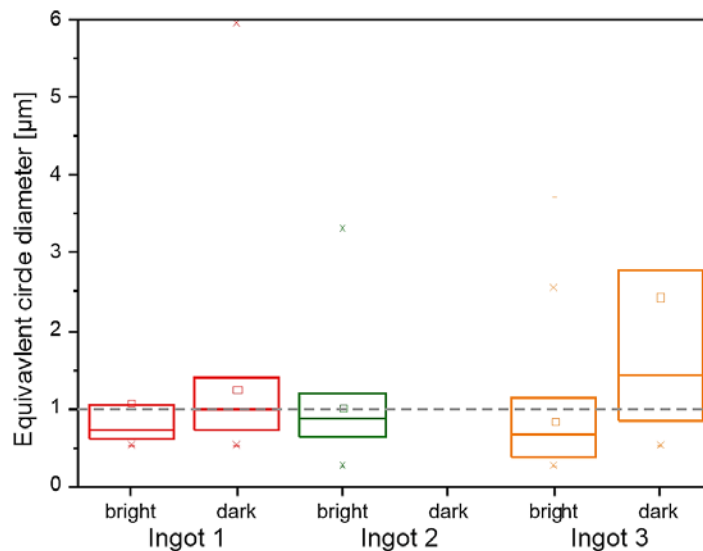


Fig. 7 - Equivalent circle diameter of bright and dark NMI

Additionally to the inclusion size the number of inclusions per mm^3 was examined. This seems to be the third important factor besides inclusion chemistry and size. It could be expected that ingot 2 has the highest inclusion density, because with a high inclusion density there are more nucleation points for the steel during solidification. Fig. 8 shows the determined inclusion densities for ingot 1 to 3, it reaches $6.8 \cdot 10^5 \text{ mm}^{-3}$ in ingot 2, while experiment 1 only contains $1.2 \cdot 10^5 \text{ mm}^{-3}$. This correlates with the macroscopic results, therefore if the inclusion density increases, the grain size decreases and the transition from columnar to equiaxed solidification takes place sooner.

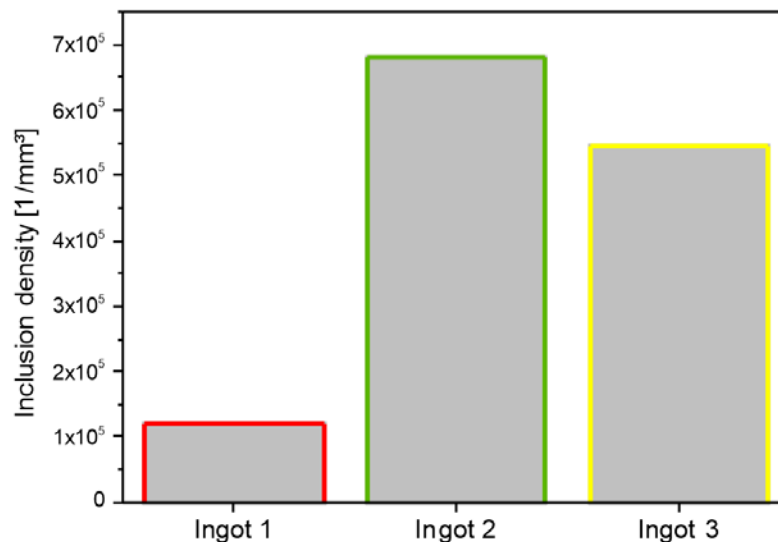


Fig. 8 - Inclusion density inside the different ingots

SUMMARY

This work confirmed the potency of cerium as a grain refiner in super austenitic stainless steel. A commercial grain refiner consisting of Fe-Cr-Si-Ce was applied in three experiments in different amounts. All experiments showed a refined macrostructure compared to a reference block cast in previous experiments [16]. The cerium amount contained in the ingots could not explain the various degrees of grain refinement in the experiments. So the next measure was to thoroughly examine the nonmetallic inclusions in the melt. As suggested by literature the NMI act as starting point for heterogeneous nucleation. In all experiments NMI were obtained with the chemical composition of CeAlO_3 . The size distribution of the inclusions shows that a large amount of the bright inclusions were smaller than $1 \mu\text{m}$ and thus were able to act as nucleation sites. The inclusion density emerged to be the most crucial factor to achieve fine grains and a large equiaxed center area. An inclusion density of about $7 \cdot 10^5$ inclusions per mm^3 led to a primary grain size of 1.2 mm and an area part of globular solidification of 76% .

ACKNOWLEDGMENT

This work was performed with support of Böhler Edelstahl GmbH & Co KG. The grain refinement alloy was provided by Elkem Foundry Products.

REFERENCES

- [1] J.C. LIPPOLD and D.J. KOTECKI, *Welding metallurgy and weldability of stainless steels*. Wiley-Interscience, Hoboken (2005).
- [2] P. MARSHALLI, *Austenitic stainless steels: Microstructure and mechanical properties*. Elsevier, London (1984).
- [3] G. GOTTSTEIN, *Physikalische Grundlagen der Materialkunde*. Springer (2007).
- [4] E. COLEMAN, D. WEINSTEIN, and W. ROSTOKER, *Acta Metall.* 9, (1961), p.491–496.
- [5] C. VAN DER EIJK, J. WALMSLEY, Ø. GRONG and O.S. KLEVAN, *59th Electric Furnance and 19th Process Technology Conferences*, Phoenix, USA (2001).
- [6] K. SCHWERDTFEGER and A. DIENER, *Metallurgie des Stranggiessens: Giessen und Erstarren von Stahl*.

Stahleisen, Düsseldorf (1992).

- [7] F. BARAKAT, Untersuchungen zur Verfeinerung des Gußgefüges von Schnellarbeitsstählen, PhD-Thesis, Montanuniversität Leoben, (1974).
- [8] B. BRAMFITT, Metall.Trans. 1, (1970), p.1987–1995.
- [9] Ø. GRONG, Metallurgical modelling of welding. The Institute of Materials (1997).
- [10] M. ANDERSSON et.al., Grain size control in steel by means of dispersed non-metallic inclusions- GRAINCONT. RCFS publications (2011).
- [11] H. SUIITO, H. OHTA, and S. MORIOKA, ISIJ Int. 46, (2006), p.840–846.
- [12] H. LI, A. MCLEAN, J.W. RUTTER and I.D. SOMMERVILLE, Metall. Trans. B 19B, (1988), p.383–395.
- [13] Y. NURI, T. OHASHI, T. HIROMOTO und O. KITAMURA, ISIJ Int. 22, (1982), p.399–407.
- [14] Y. NURI, T. OHASHI, T. HIROMOTO, and O. KITAMURA, ISIJ Int. 22, (1982), p.408–416.
- [15] N. KOJOLA, S. EKEROT, M. ANDERSSON and P. G. JÖNSSON, Ironmaking Steelmaking 38, (2011), p.1–11.
- [16] R. KOLOSZAR, Kornfeinung hochlegierter Stähle durch heterogene Keimbildung, Master-Thesis, Montanuniversität Leoben, (2014).